High temperature reaction kinetics of CN(v = 0) with C2H4 and C2H6 and vibrational relaxation of CN(v = 1) with Ar and He

Ghassen Saidani, Yulia Kalugina, Aline Gardez, Ludovic Biennier, Robert Georges, François Lique

High temperature reaction kinetics of CN($v = 0$) with C_2H_4 and C_2H_6 and vibrational relaxation of CN($v = 1$) with Ar and He

Ghassen Saidani[1], Yulia Kalugina[2,3], Aline Gardez[1], Ludovic Biennier[1*], Robert Georges[1] and François Lique[2†]
[1] *Institut de Physique de Rennes, Département de Physique Moléculaire, Astrophysique de Laboratoire, UMR CNRS 6251, Université de Rennes 1, Campus de Beaulieu, 35042 Rennes Cedex, France*
[2] *LOMC - UMR 6294, CNRS-Université du Havre, 25, Rue Philippe Lebon, BP 540, 76058, Le Havre, France*
[3] *Department of Optics and Spectroscopy, Tomsk State University, 36 Lenin av., Tomsk 634050, Russia*
(Dated: Received 22 December 2012 ; accepted 27 February 2013)

The investigation of the chemical complexity of hot environments, ranging from combustion flames to circumstellar envelopes of evolved stars, relies on the determination of the reaction kinetics and product branching ratio. We have designed a chemical reactor for the exploration of high temperature chemistry. This apparatus, is employed in the present study to measure the reaction kinetics of the CN radical with C_2H_4 and C_2H_6 over the 300 –1200 K temperature range. In our setup and in some environments, the CN radical is partially produced in a vibrationally excited state, before relaxing by collision with the surrounding gas. We complement the experimental kinetic studies of hydrocarbons reactions with CN($v = 0$) with a theoretical study of vibrational relaxation of CN($v = 1$) by He and Ar atoms, the main collisional partner in our apparatus. Calculations are carried out to determine the collisional elastic and inelastic cross sections versus the kinetic energy as well as the corresponding vibrationally elastic and inelastic rate coefficients. The results are compared with empirical calculations and with a few experimental observations. The range of validity of the empirical model is discussed and potential applications sketched.

INTRODUCTION

Free radicals play a major role in flame chemistry because of their high reactivity. The investigation of the chemistry of species such as OH, CH, C_2H or CN is necessary to understand the formation and destruction of combustion generated pollutants and soot particles. The CN radical is a key molecular species in the nitric oxide (NO) chemistry cycle [1], which is itself the predominant NO_x species formed in combustion. The reaction of atmospheric N_2 with CH or the combustion of nitrogen-containing fuels generate HCN. Once produced, HCN can either directly react with OH to form CN or can partially convert to NO through a series of reactions. NO can then react with atomic C to give CN. The absolute concentrations of the CN radical have recently been established in methane/air low pressure flames (33 mbar $\leq P \leq$ 53 mbar) by cavity ringdown spectroscopy [2, 3]. The two independent studies reported a peak concentration at the 10^9 molecule·cm^{-3} level (tens of ppb). Although already significant, this value increases by one order of magnitude for NO-seeded CH_4/O_2 low pressure flames as reported by studies employing laser induced fluorescence calibrated by Rayleigh or Raman scattering [3].

Combustion flames are not the only hot environments in which the CN radical is detected and plays a significant role in molecular complexity. In particular, this molecular species has been observed in more than forty circumstellar envelopes of evolved stars [4], including IRC +10216, the closest dying star [5]. Presently, more than 75 species have been identified in those environments [6], with half of them only in IRC+10216. The vast majority of the detected molecules are carbon rich species. Acetylene, C_2H_2, observed in absorption in the 3.3 μm and in the 11–14 μm mid-infrared regions represents the most abundant hydrocarbon. Ethylene, C_2H_4, has also been observed although at a lower abundance [4]. About one third of the identified species are made both of carbon and nitrogen. This includes hydrogen cyanide, HCN, which is one of the most abundant species after H_2, He, H and CO, at a level comparable to acetylene C_2H_2. Astronomical observations reveal that HCN is ubiquitous but concentrated near the star [7]. The interstellar UV radiation penetrates deeply into the envelope because of its clumpy structure and dissociates HCN to give the cyanide radical, CN, which is observed in the outer layers. The models reproduce reasonably well the ratio of peak CN abundance over initial HCN abundance. Larger carbon and nitrogen bearing molecules have been identified such as cyanopolyynes from HC_2N to HC_9N with HC_3N detected in 9 other sources [4]. Their abundance can reach very high values up to 10^{-6} with respect to H_2. The reaction of CN with hydrocarbon chains is considered as the dominant formation channel of cyanopolyynes at low temperature [8]. The models developed to understand the rich chemistry of these media rely on the knowledge of relevant chemical processes which are only partially known. In particular, the reaction of CN with a selection of hydrocarbons exhibits a variety of tem-

*Electronic mail: ludovic.biennier@univ-rennes1.fr
†Electronic mail: francois.lique@univ-lehavre.fr

perature dependencies and products (see Ref. [9] and references therein) that deserve investigation.

In our laboratory, we have designed a chemical reactor for the exploration of high temperature chemistry. This apparatus has been recently employed to measure the reaction kinetics of the CN radical with propane, propene, allene, 1,3-butadiene and 1-butyne over the 300–1200 K temperature range [9]. We use it in the present work to pursue the investigation of the reaction kinetics of CN with C_2H_4 and C_2H_6 over the same temperature range.

Past studies have also revealed the existence of vibrationally excited species in the reactor. These works did not address though the chemistry and physics of these excited radicals. The kinetics of a reaction can be sensitive to the initial energy of the reactants depending on which form it is stored in the molecule. Studies on vibrationally mediated chemistry aim at opening the way for molecule-specific control of reaction pathways via spectroscopic excitation of a particular vibrational mode. Early experimental work from Sims *et al.* [10] showed that in the case of the reaction of CN($v = 1$) with e.g. H_2, there was, however, no significant enhancement of the reaction rates on vibrational excitation of CN, in agreement with the predictions of vibrationally adiabatic transition-state theory. The internal energy available in vibrationally excited CN molecules *cannot* be used to overcome the activation barrier. Similar findings were made by Sims & Smith [11] for the reaction of CN($v = 1$) with HCl, HBr, and HI.

Excited molecular species are encountered in a number of environments. For instance, strong deviation from the Maxwell Boltzmann equilibrium for the populations of the $v = 0$ and $v = 1$ vibrational levels of OH($X^2\Pi_i$) radicals were observed in the preflame zone of the methane/oxygen/nitrogen flame by cavity ringdown spectroscopy [12]. More recently, an experimental study employing vacuum ultraviolet photoionization mass spectrometry suggested the presence of vibrationally excited propargyl C_3H_3 in a low pressure fuel/O_2/Ar premixed flame [13]. Vibrationally excited species may also be found in fast flow reactors employed for kinetics studies. In some of these reactors, the radical is produced by photolysis of a molecular precursor. This method generates radicals with excess energy which cannot always be removed through collisions with the carrier gas (usually He, Ar or N_2) within the time-frame of the experiment (see e.g. [11]).

Farther from us, a number of vibrationally excited molecules have been detected in hot astrophysical environments. They include CO [14, 15], CS [16, 17], SiS [18], C_2H_2 [e.g. 19], HCN (See [20] and references therein) and C_2H [21] in IRC +10216. The contribution of vibrational excited species to the sub-millimeter wave spectrum is greater than that of isotopologues. As a consequence, these molecules may serve as probes of local physical conditions. For instance, the analysis of hot HCN has recently been used to investigate the dust formation zone of the envelope of IRC +10216 [20]. According to Cernicharo *et al.*[20], the populations of the vibrationally excited species in this environment are likely to be controlled by the interstellar, stellar, and hot dust radiations in the outer shells except if shocks, induced by pulsations of the star, end up playing a major role there. In Ori(KL), astronomical observations show that the vibrational energy distribution of HCN departs from Maxwell-Boltzmann equilibrium because of infrared pumping [16].

Back in the laboratory, and under our experimental conditions, we probe the evolution of the CN($v = 0$) population in presence of a known excess of co-reagent. The radicals are generated instantaneously at $t = 0$ by photolysis. In absence of additional source terms, the CN($v = 0$) population simply decays at a rate given by the kinetics of the reaction with the co-reagent. However, the possible relaxation of vibrationally excited CN radicals, which have been identified in the laser induced fluorescence (LIF) spectrum, could represent a source term of CN($v = 0$). As a consequence, the evolution of the population of CN($v = 0$) could not be treated as an exponential decay anymore. Even if the replenishment of the CN($v = 0$) population happens to be small, it would affect the decay and underestimate the rate coefficient.

From a fundamental viewpoint, finally, the question of the vibrational relaxation of small radicals justifies our efforts. The experimental study of the kinetics of a selection of reactions with CN($v = 0$) (Section II) is therefore complemented with a theoretical study of vibrational relaxation of CN($v = 1$) by He and Ar atoms, some of the main collisional partners in such experiments (Section III). High level calculations are carried out to determine the collisional elastic and inelastic cross sections versus the kinetic energy as well as the vibrationally elastic and inelastic rate coefficients. The results are compared with empirical calculations and with a few experimental and astrophysical observations. The range of physical and chemical conditions under which the relaxation of vibrationally excited radicals may play some role is equally studied (Section IV), and the direct consequences on the current work examined.

LABORATORY EXPERIMENTS

Experimental apparatus

The kinetic experiments are performed in a unique high temperature chemical reactor which combines a high enthalpy source with a flow tube and a PLP-LIF (Pulsed Laser Photolysis - Pulsed Laser Induced Fluorescence) system to probe the undergoing chemical reactions. The high enthalpy source is a powerful heat exchanger (because of the huge exchange surface) made of a resistively heated porous graphite rod. The source was origi-

nally combined with a FTIR spectrometer to record the emission spectrum of hot gases such as acetylene and methane [22, 23]. Incidentally, it was also employed to produce carbonaceous particles under certain operating conditions [24]. More recently, the source has finally been adapted to measure the kinetics of reactions of interest for hot atmospheres [9]. Each of the components of the reactor and their functions were detailed in the former paper [9]. The buffer gas contained in a high-pressure reservoir ($P_{\rm res} \sim 600$ mbar) is heated up by traveling through the hot porous walls of the graphite rod, before ending its course in the rod cavity. The gas is then evacuated into a 38 mm flow tube in which a low pressure ($P_{\rm ch} \sim 4-5$ mbar) is maintained by a Roots pump. Two capillaries are set up downstream the nozzle for the injection of the vapors of the radical precursor ICN ($P_{\rm vap}^{\rm sat} \sim 1.3$ mbar), whose crystals are deposited in an independent flow cell ($P \sim 160$ mbar) and entrained by a small Ar flow ($Q_{\rm Ar} \sim 300$ standard cm^3·min^{-1}). Under these conditions, the density of ICN in the flow ends up around $n_{\rm ICN} \sim 10^{12}$ molecule·cm^{-3}. The insertion of a tungsten grid a few centimeters further downstream the nozzle slows down the flow converting the kinetic energy back into enthalpy. It also promotes a good mixing of the vapors with the carrier gas. The flow is probed before the hydrodynamic entrance length, in the region not perturbed by the boundary layers, where the heat exchange between the gas and the wall of the flow reactor is negligible. During our experimental measurements, the mass flow rate was chosen high enough (~ 15.8 standard l·min^{-1}) to provide a high entrance length about 10 to 15 centimeters beyond the probing zone.

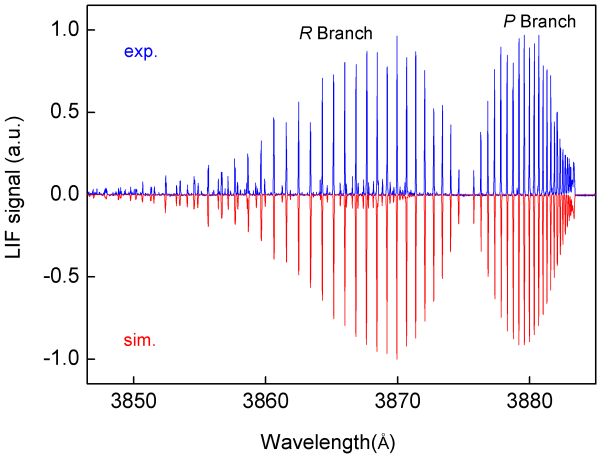

FIG. 1: Top: experimental LIF spectrum of the $B^2\Sigma^+ \leftarrow X^2\Sigma^+$ transition of the CN radical produced by the 266 nm photolysis of ICN in a Ar flow (15.8 slm) measured for a delay $\Delta t = 30$ μs. Bottom: simulated non-saturated LIF spectrum of the CN radical at the rotational temperature of 483 K and the vibrational temperature of ∼1400 K with a gaussian instrumental profile with a full width at half maximum of 0.045 Å using the LIFBASE program [25].

Production of CN($v = 0, 1$)

The cyano radicals are generated coaxially to the flow reactor by the photolysis of cyanogen iodide (ICN, Aldrich 95%) at the wavelength of 266 nm provided by a pulsed Nd:YAG laser (Spectra Physics GCR 190 operating at 10 Hz) with a fluence $\mathcal{F} \sim 50$ mJ·cm^{-2}. A non-negligible percentage of CN population is generated in the $v = 1$ state (see e.g. Ref. [26]). The concentration of CN can be estimated around 3×10^{10} molecule·cm^{-3} under our experimental conditions using the following formula:

$$n_{\rm CN} = \phi(\lambda)\ \Delta t\ \sigma_{\rm abs}(\lambda)\ n_{\rm ICN}\ \eta \qquad (1)$$

with $\sigma_{\rm abs}(\lambda) \sim 3 \times 10^{-19}$cm^2, the ICN absorption cross section at $\lambda = 266$ nm[27], $\Delta t \sim 8$ ns the irradiation time, $\eta \sim 1$ the dissociation quantum yield, and $\phi(\lambda) = \mathcal{F}/(\Delta t \cdot h\nu)$ the UV photon flux. Cyano radicals are monitored by LIF. A nanosecond dye laser (ND6000 Continuum, 10 Hz, 4 mJ/pulse at $\lambda_{\rm exc} \sim 385$ nm) pumped by a third harmonic of a Nd:YAG laser (GCR 230, Spectra-Physics, 10 Hz, 60 mJ/pulse at 355 nm) is employed as the excitation source. The evolution of the population of CN is probed by collecting the fluorescence light out-of-resonance at $\lambda_{\rm fluo} \sim 420$ nm with the help of a 10 nm bandpass filter and by varying the delay between the photolysis pulse and the excitation pulse. Usually, the laser is tuned to the more intense line of the R branch ($7 \le J \le 13$). The experimental LIF spectrum displayed on Figure 1 shows clearly two weak bands, assigned to the (1-1) hot band transition. From the determination of the integrated intensity of these features and of the (0-0) cold band, we estimate that ∼10% of the CN radicals are in the $v = 1$ state. This value corresponds to a vibrational temperature of ∼1400 K.

The evolution of the CN radical in the $v = 0$ and $v = 1$ states, represented on Fig. 2 is probed by tuning the laser to the $(0-0)R(13)$ and $(1-1)P(2)$ lines, respectively. The two curves unambiguously trace back to a very similar history. Apart from the spike of the signal at 0 μs which originates from scattered excitation photons, we clearly distinguish two regimes. Over the 0-250 μs time interval, the signal decays slowly at a rate of $\sim 1800 \pm 200$ s^{-1} and $\sim 1500 \pm 350$ s^{-1} for the CN($v = 0$) and CN($v = 1$) respectively. This signal loss, due to diffusion, is consistent with results obtained using Fick's law. The calculations of the diffusion of CN in a Ar buffer gas performed for a 8 mm-diameter radical column in a 38 mm diameter cylinder and with a diffusion coefficient of $D = 175$ cm^2·s^{-1} show that after 250 μs, one third of the radicals have been lost by diffusion. The grid positioned 82 mm upstream the probe region is responsible for the regime change that occurs at 250

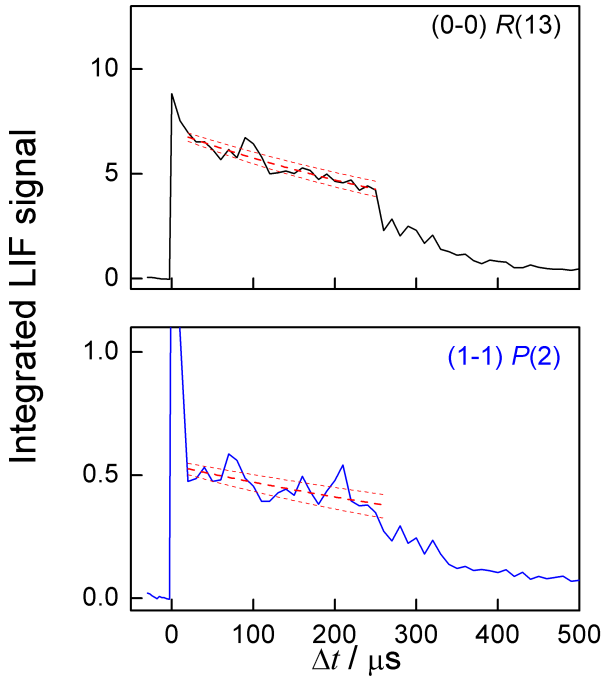

FIG. 2: Experimental Integrated LIF signal of the CN ($v = 0$) (−) and CN ($v = 1$) (−) at $T_R = 680$ K in Ar (15.8 slm) in absence of co-reactant.

μs. Incidentally, it can be used to estimate the central flow velocity $v_m \sim 326$ m·s^{-1}. This value corresponds to an average velocity of 163 m·s^{-1}, in good agreement with calculations from the conservation of mass flow rate $Q_m = \rho\langle v\rangle S$, with ρ the density calculated from the pressure and the temperature, $\langle v\rangle \sim 158$ m·s^{-1}, the average flow velocity and S the flow section. Computational flow dynamics calculations are under way to examine the details of the flow and the exact role of all the components. Above a delay of 250 μs, we probe parcels of gas upstream the grid. In that region, the gas is heavily mixed and its history scrambled. According to Figure 2, there is no obvious transfer from the $v = 1$ to the $v = 0$ state within the hydrodynamic time of 250 μs of the experiment which would translate into a faster decay of the CN($v = 1$) signal at the benefit of the CN($v = 0$) signal. Theoretical calculations of vibrational relaxation performed below will permit to explore the full range of conditions under which vibrational relaxation could play some role.

Kinetic experimental procedure

The details of the experimental procedure to measure the reaction kinetics are mentioned in a former paper [9]. Rate coefficients are determined under pseudo-first-order conditions assuming that the concentration of CN radical is much smaller than the reagent concentration [C_nH_m].

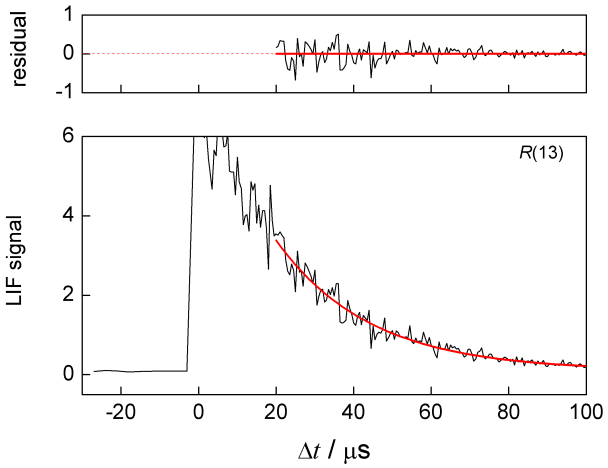

FIG. 3: Experimental LIF signal (−) of the CN radical at $T_R = 483$ K in Ar (15.8 slm) in the presence of [C_2H_6]=104 × 10^{13} molecule · cm^{-3} and the fitting curve (−).

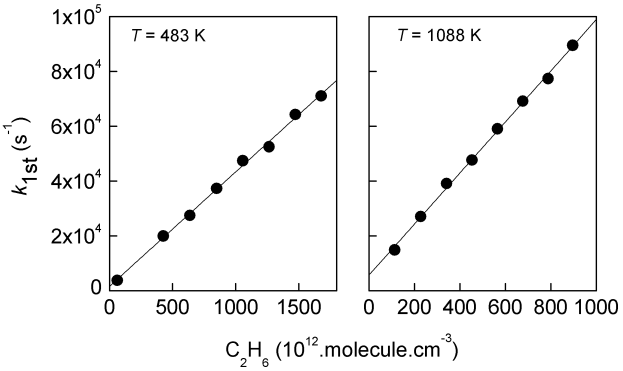

FIG. 4: Second order plots for the reaction between the CN radical and C_2H_6 for $T_R = 483$ K and $T_R = 1088$ K.

Figure 3 represents an example of LIF signal decay of CN radical in the presence of [C_2H_6]=104 × 10^{13} molecule · cm^{-3} in Ar at $T_R = 483$ K. The residual curve is also plotted in order to verify the exponential nature of the decay and identify any contribution of the vibrational excitation on longer time scale. In order to probe a spatial region thermally uniform, we consider only the first 100 μs, corresponding to a few centimeters. This procedure is repeated for different concentrations of reactant. We plot then k_{1st} versus [C_nH_m] (Figure 4) which varies linearly with k_{2nd} as the slope. The rate coefficient of the reaction at a given temperature is obtained by linear regression of the experimental curve by the method of least squares.

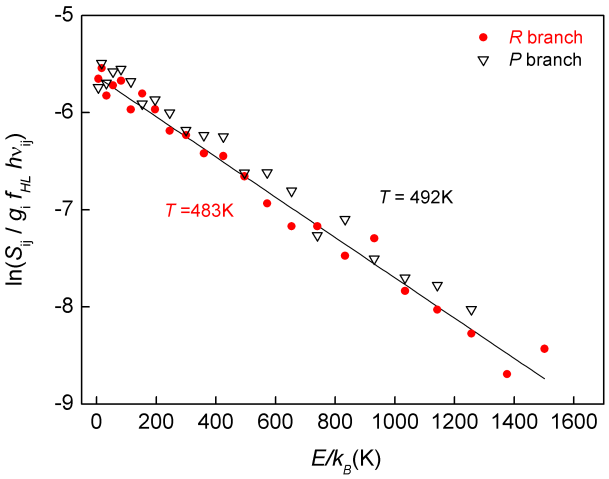

FIG. 5: Boltzmann plot derived from the analysis of the LIF spectrum displayed in Figure 1.

Gas Temperature

The gas rotational temperature is derived from the analysis of the LIF spectrum, such as one shown in Figure 1, using a Boltzmann plot. This procedure is systematically used to extract the rotational temperature of the gas flow for electrical currents applied to the porous graphite rod varying from 0 to 130 A, corresponding to a range of temperature between 298 and 1200 K. The line intensity S_{ij}, corresponding to the transition between levels i and j, of energy E_i and E_j, is proportional to $g_i f_{HL} h\nu_{ij} \exp(-E_i/k_B T)$ with g_i the degeneracy of the lower energy level, f_{HL} the Hönl-London factor which equals J and $J+1$ for the $P(J)$ and $R(J)$ lines respectively, $h\nu_{ij} = E_j - E_i$ the energy difference between the two levels, and k_B the Boltzmann constant. The plot of the semi-logarithm of $S_{ij}/(g_i f_{HL} h\nu_{ij})$ against the energy of the lower level E_i/k_B, is a straight line with a slope $-1/T$ which directly gives the temperature. Only the R branch was eventually considered because of strong line overlap in the P branch. The plot describes the extraction of the temperature from only one spectrum. Two to four of them where accumulated to reduce the uncertainty, which comes to ±10 to 30 K for a 95% confidence interval. The uncertainty could certainly be reduced in future experiments by (1) further averaging, and by (2) better handling the line intensity integration in crowded spectral regions.

CN+C$_2$H$_6$

The kinetics of the reaction of CN ($X^2\Sigma^+$) with ethane (C_2H_6) is explored over the 300-1120 K temperature range and the global rate coefficient is reported on Table I. The quoted uncertainties include both statistical and systematical errors. The statistical error is calculated as the product of the standard error from the fit of the second-order rate coefficient plot and the appropriate Student's t factor for the 95% confidence limit. The systematic error, estimated to 10%, originates mainly from the inaccuracy in the calibration of the flow controllers and from the determination of the total number density. The rate coefficient of this reaction is moderately fast (few 10^{-11} cm$^3\cdot$ molecule$^{-1}\cdot$ s^{-1}) at room temperature before increasing with temperature (See Figure 6). This is consistent with the fact that ethane is a saturated hydrocarbon (alkane). It is composed of stable σ type bonds much less reactive than that of the unsaturated hydrocarbons such as alkenes or alkynes with electrons of π orbitals. The reaction of CN with ethane may be modeled over the 300−1200 K temperature range by a modified three parameters Arrhenius law:

$$k(T) = A(298\text{ K})(T/298)^n \exp(-\theta/T) \qquad (2)$$

where $A(298\text{ K}) = 3.5 \times 10^{-12}$ cm$^{-3}\cdot$ molecule$^{-1}\cdot$ s^{-1}, with $n = 2.16$ and $\theta = -624$ K. The results of this study are in good agreement with earlier work of Herbert *et al.* [30], Balla *et al.* [31] and Yang *et al.* [28] showing a pronounced temperature dependence. In their studies of the reaction kinetics of the CN radical with various

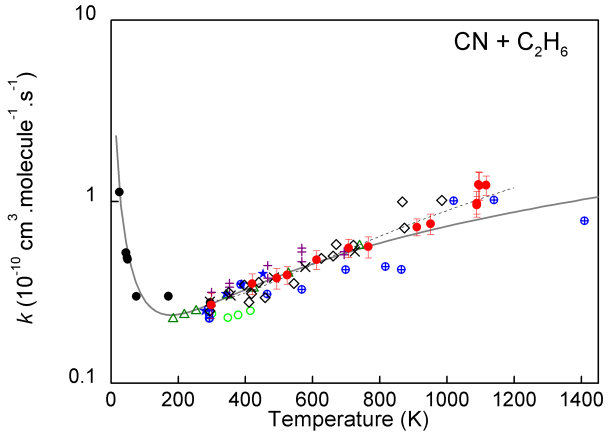

FIG. 6: Rate coefficients for the reaction of CN($X^2\Sigma^+$) with ethane, C_2H_6, as a function of temperature. This work: (●). Yang *et al.* [28] between 185 and 739 K: (△). Hess [29] over the 294 –736 K range: (×). Herbert *et al.* [30] over 297 – 694 K range: (+). Balla *et al.* [31] using PLP-LIF and diode absorption spectroscopy over the 292 –1409 K : (⊕). Copeland *et al.* [32] over the 279 –452 K range: (⋆). Atakan *et al.* [33] over the 294-984 K : (◇). Bullock *et al.* [34] over the 300 –415 K range: (○). Sims *et al.* using a supersonic uniform flow reactor (CRESU) [35] : (•). The full line represents theoretical calculations by Georgievskii and Klippenstein [36] over the 20 –1140 K range combining VRC-TST and 2TS. The dotted line correspond to the fit of our data over the 298 –1116 K range.

hydrocarbons including C_2H_6 and C_2H_4, Sims *et al.* [35] discussed the behavior of the reaction rates with the gas temperature down to 25 K. They suggested a mechanism involving the formation of a van der Waals complex at low temperature. In order to model the phenomenon Georgievskii and Klippenstein [37] developed a theoretical approach based on two transition states (2TS). They considered that the reaction of CN with ethane was a good test to validate the functionality of this model because the reaction proceeds by a mechanism of hydrogen abstraction (H-abstraction) without stabilization of reaction intermediates :

$$CN + C_2H_6 \rightarrow C_2H_5 + HCN \quad (3)$$

Indeed, no pressure dependence on the temperature range studied was observed for this reaction [30]. This behavior as a function of temperature is due to the high electron affinity of the CN radical (∼3.82 eV) that can tear easily one H of the hydrocarbon. This approach has also been used to model the kinetics of reaction between OH and C_2H_4 (ethylene) [38] as discussed in Section III. A comparison between model and experiments is given for the reaction between CN and C_2H_6 in Figure 6. The 2TS model [37] reproduces remarkably well the experimental trend in the reaction of CN with ethane at low temperatures (∼ 200 K). At higher temperature, as shown in Figure 6, it is rather a model based on calculations of type variational reaction coordinate - transition state theory (VRC-TST) that best fits our experimental results. This work further strengthens the influence of the 2TS theory coupled to the VRC-TST method to explain this behavior.

Some independent measurements above 1150 K are however needed to confirm the leveling off of the rate coefficient suggested by the unique data-point at 1400 K reported by Balla *et al.* [31].

CN+C$_2$H$_4$

In this work, we report for the first time, the global reaction rate coefficient for CN with ethylene (C_2H_4) above 750 K. Table I gathers the kinetics data over the 298–1116 K temperature range. Reactions of CN with unsaturated hydrocarbons have been significantly less studied than with saturated species. They are usually fast because their π-type bonds made up of electrons on π orbitals are quite reactive. The reaction of CN with ethylene fulfills this rule (k ≥ 10^{-10} cm^3· molecule^{-1}· s^{-1}) and can be modeled over the 298–1116 K range by an Arrhenius law following Eq. 1 using $A(298\ \mathrm{K}) = 6.0\times10^{-11}$ cm^{-3}· molecule^{-1}· s^{-1}, with $n = 0.65$ and $\theta = -401$ K. The reaction of CN with ethylene can take place along the two main channels [39]:

$$CN + C_2H_4 \rightarrow ... \rightarrow H_2C{=}CH(CN) + H \quad (4)$$

TABLE I: Rate coefficients of the CN+C_2H_4 and CN+C_2H_6 reactions.

C_2H_6			
T^a /K	M	[R] /10^{13} molec.·cm^{-3}	k_{2nd} /10^{-11} cm^3· molec.$^{-1}$· s^{-1}
298 ±5	Ar	17.1- 34.4	2.69±0.42
420 ±10	N_2	24.3-213.05	3.53±0.46
483 ±15	Ar	22.8-201.7	3.78±0.49
524 ±20	Ar	20.8-184.7	3.93±0.43
611.5 ±15	Ar	17-150.6	4.78±0.57
707 ±20	Ar	0.35-9.6	5.55±0.64
765 ±25	Ar	15.3-135.5	5.64±0.75
910 ±25	Ar	11.8-104.7	7.24±0.78
951 ±25	Ar	11-97.7	7.54±0.96
1088 ±25	Ar	11.3-100.6	9.79±1.57
1093 ±30	Ar	10.8-95.8	12.43±2.13
1096 ±25	Ar	9.07-80.32	12.26±2.2
1116 ±30	Ar	7-62.5	12.32±1.48
C_2H_4			
T /K	M	[R] /10^{13} molec.·cm^{-3}	k_{2nd} /10^{-10} cm^3· molec.$^{-1}$· s^{-1}
298 ±5	Ar	0.9- 47.75	2.35±0.28
420 ±10	N_2	2.55-27.9	1.90±0.24
483 ±15	Ar	3.06-27.96	1.78±0.27
524 ±20	Ar	2.8-25.6	2.0±0.25
611.5 ±15	Ar	2.3-21	1.82±0.23
707 ±20	Ar	0.98-14.9	1.79±0.23
765 ±25	Ar	2.1-18.8	1.76±0.24
910 ±25	Ar	1.6-14.6	1.99±0.25
951 ±25	Ar	1.6-14.52	2.2±0.25
1088 ±25	Ar	1.58-14.38	2.08±0.26
1093 ±30	Ar	1.53-13.96	1.94± 0.27
1096 ±25	Ar	1.46-13.3	1.86±0.247
1116 ±30	Ar	1.11-10.12	2.03±0.4

[a]The rotational temperature is determined from the *R* branch which exhibits fewer overlapping lines

or

$$CN + C_2H_4 \rightarrow ... \rightarrow HCN + C_2H_3 \quad (5)$$

with both having separate transition states.

The latest theoretical work performed at the CCSD/aug-cc-pVDZ level gives relative energies of −67 and −57 kJ/mol for the H and the C_2H_3 formation channels, respectively [40]. According to that study, there are two pathways that lead to H production (4). About 20% of all initial collision complexes show C-H bond rupture via a tight exit transition state located 21 kJ/mol above the products to form vinylcyanide, C_2H_3CN, and atomic hydrogen. The remaining 80% undergo an H atom shift via a 163 kJ/mol well to yield CH_3CHCN prior to an H atom release and formation of vinylcyanide. Reaction (5) leading to HCN + C_2H_3 proceeds through a transition state located 18 kJ/mol above the reactants.

The direct observation of the reaction product C_3H_3N was made by Monks *et al.* [41] in a quadrupole mass spectrometry by electron impact in a low pressure discharge by analyzing the branching ratio of reaction products.

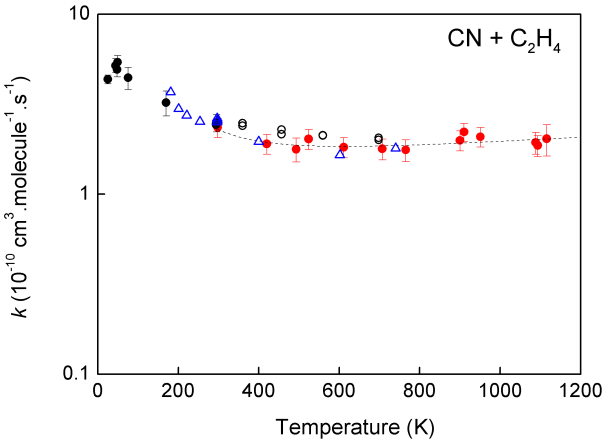

FIG. 7: Rate coefficients for the reaction of CN($X^2\Sigma^+$) with ethylene, C_2H_4, as a function of temperature. The filled red circles (•) represent the experimental results obtained with the high temperature flow tube. The empty blue triangles (△) correspond to the data obtained by Yang *et al.* [28] between 181 and 740 K whereas the black empty circles (○) were measured by Herbert *et al.* [30] using a flow tube/PLP-LIF apparatus over the 295–698 K range. Finally, the black full circles (●) represent measurements performed by Sims *et al.* using a supersonic uniform flow reactor (CRESU) [35]. The dotted line correspond to the fit of our data over the 298-1116 K range.

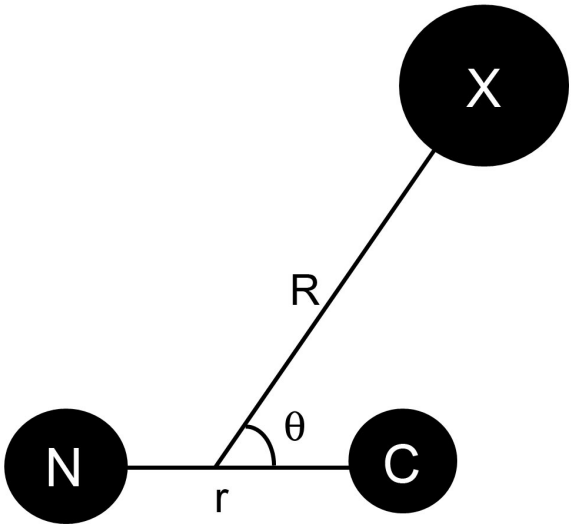

FIG. 8: Coordinate system of the CN - X (X = He, Ar) complex.

Balucani *et al.* [42] investigated later the dynamics of this reaction via a system of crossed molecular beams coupled to mass spectrometry angularly resolved at collision energies of 15.3 and 21 kJ/mol. They showed that the reaction has no entrance barrier and is initiated by addition of CN($X^2\Sigma^+$) to the π electron density of the olefin to give a long-lived CH_2CH_2CN intermediate.

Using another experimental configuration based on a slow flow/flash photolysis setup, Choi *et al.* [39] determined a branching ratio of H produced by the reaction (4) by VUV-LIF technique in its series Lyman α (∼121.6 nm) close to unity. This measurement was confirmed by the simultaneous observation of the decrease of the signal of the CN radical. They therefore concluded that at room temperature, the reaction is governed by a mechanism of addition / elimination with a hydrogen replaced by CN [39]. This mechanism was first proposed by Lichtin *et al.* [43] and Herbert *et al.* [30] employing PLP-LIF, showing also at the time that the CN+C_2H_4 reaction was independent of the total pressure.

We have shown that the CN radical can react very efficiently with small hydrocarbons. In a variety of environments but also from a fundamental viewpoint, it is important to determine the vibrational state of the reactants. In the following section, we complement the experimental kinetic studies of hydrocarbons reactions with CN($v = 0$) with a theoretical study of vibrational relaxation of CN($v = 1$) by He and Ar atoms, the main collisional partners in our apparatus. The evolution of the CN radical in the $v = 0$ and $v = 1$ states is a key parameter of the experimental determination of the reactive rate coefficients. In our experiments, we have seen that there is no transfer from the $v = 1$ to the $v = 0$ state within the hydrodynamic time of 250 μs of the experiment. However, quantum calculations of vibrational relaxation, described below, will permit to explore the range of conditions under which vibrational relaxation could play some role. At the end of the following section, the quantum calculations will be compared with the results obtained with a very accessible empirical model.

THEORETICAL APPROACH FOR THE RELAXATION OF CN($v = 1$)

Ab initio calculations

In the present work, we use the Jacobi coordinate system presented in Figure 8. The origin is the center of mass of the CN molecule and vector **R** connects the center of mass of CN molecule and atom X (He or Ar). The rotation of CN molecule is defined by the θ angle. The interatomic distance of the CN molecule is designated as r.

Ab initio calculations of the potential energy surface (PES) of van der Waals complexes CN–X being in their ground electronic states ($^2\Sigma^+$, or $^2A'$ in C_s symmetry group) were carried out at the SAPT(DFT) level of theory for open-shell systems [44] implemented as an extension of the SAPT2008 [45] package. We have used a hybrid density functional PBE0 [46] which was proved to lead to the most accurate results for closed-shell systems [47, 48], and has been successfully used in SAPT(DFT)

calculations for open-shell systems [44].

To achieve a good description of the charge-overlap effects, the calculations were performed in dimer-centered basis set using additional midbond functions ($DC^{+}BS$ approach [49]). In the present work, Dunning's augmented correlation-consistent triplet zeta (aug-cc-pVTZ) basis set [50] augmented by the (3s 3p 2d 2f) midbond functions [51] was used.

The calculations were carried out for five r-distances: 1.85, 2.05, 2.21, 2.4 and 2.6 bohr, for Jacobi angle θ from 0° to 180° with the step of 15° and for R-distances from 3.0 to 25 bohr for CN-He (2455 geometries) and from 4.5 to 25 bohr for CN-Ar (2078 geometries).

In SAPT(DFT) method based on Kohn-Sham (KS) density functional theory, the interaction energy (up to the second order) is expressed as a sum of the interaction energy components [48]:

$$\begin{aligned} V &= E^{(1)}_{elst}(\mathrm{KS}) + E^{(1)}_{exch}(\mathrm{KS}) + E^{(2)}_{ind}(\mathrm{CKS}) \\ &+\tilde{E}^{(2)}_{exch-ind}(\mathrm{CKS}) + \tilde{E}^{(2)}_{exch-disp}(\mathrm{CKS}) \\ &+E^{(2)}_{disp}(\mathrm{CKS}), \end{aligned} \tag{6}$$

where CKS stands for coupled-KS method of computing the response properties [48].

The accuracy of the CN–He PES was improved by scaling the interaction energy components by a fixed amount [52]. We have scaled both the dispersion and exchange parts of the potential V (Eq. 6) by factors:

$$\begin{aligned} V^{\text{CN-He}} = & \quad E^{(1)}_{elst} + 0.935E^{(1)}_{exch} + E^{(2)}_{ind} \\ & +\tilde{E}^{(2)}_{exch-ind} + 0.87(\tilde{E}^{(2)}_{exch-disp} + E^{(2)}_{disp}) \end{aligned} \tag{7}$$

Reference energies were taken from Ref. [53].

For the case of CN-Ar complex, bad perfomance of S^2 approximation [54] at small and medium intermolecular separations was found. Hence, we have scaled exchange-induction and exchange-dispersion terms in Eq. 6 [55] as:

$$\begin{aligned} V^{\text{CN-Ar}} &= E^{(1)}_{elst} + E^{(1)}_{exch} + E^{(2)}_{ind} + E^{(2)}_{disp} \\ &+E^{(20)}_{exch-ind}E^{(1)}_{exch}/E^{(1)}_{exch}(S^2) + \\ &E^{(20)}_{exch-disp}E^{(2)}_{disp}/E^{(20)}_{disp}. \end{aligned} \tag{8}$$

The potential $V(r, R, \theta)$ was fitted to the functional form [56]:

$$V(r, R, \theta) = \sum_{n=1}^{N_{max}} \sum_{l=1}^{L_{max}} d^{l+m-1}_{m,0}(\cos\theta) A_{ln}(R)(r - r_e)^{n-1} \tag{9}$$

where the $d^{l+m-1}_{m,0}(\cos\theta)$ are reduced Wigner rotation matrix elements.

N_{max} equals the number of CN bond distances, L_{max} equals the number of angles θ for which the potential was calculated and m=0.

For a vibrational Close-Coupling rotational Infinite Order Sudden method (VCC-IOS) [57], that will be used to perform the scattering calculations, matrix elements of the potential between the vibrational states of the CN molecule are required for fixed values of the Jacobi scattering angle and for all the R-values. We write these matrix elements as:

$$V_{v,v'}(R, \theta) = \langle v(r) \mid V(r, R, \theta) \mid v'(r) \rangle \tag{10}$$

The CN vibrational wave functions $\mid v'(r)\rangle$ were evaluated by the Fourier Grid Hamiltonian (FGH) method of Clay Marston & Balint-Kurti [58] from a CN potential calculated with a RKR program [80]. The vibrational wave functions were taken with $j = 0$.

Figure 9 shows a contour plot of the CN–He and CN–Ar $V_{0,0}(R, \theta)$ potential energy matrix element for vibrationally elastic scattering as a function of R and θ variables. This matrix element displays the same basic features than the 2D PES obtained for these collisional system at fixed intermolecular distance (see Figure 1 of Ref. [53] and Figure 7 of Ref. [59]). One can note that the $V_{1,1}(R, \theta)$ matrix element of the CN–He (upper panel) and CN–Ar (lower panel) interaction potentials is very similar to the $V_{0,0}(R, \theta)$ ones.

Figure 10 shows a contour plot of the CN–He and CN–Ar $v = 0 \rightarrow v' = 1$ potential energy matrix element for vibrationally inelastic scattering as a function of R and θ variables. The plot shows, as would naturally be expected, that the coupling of the $v = 0$ and $v = 1$ levels increases as the scattering coordinate R decreases. However, the coupling between different vibrational levels is small in comparison with the coupling between identical vibrational levels.

Scattering calculations

We have used the VCC-IOS approximation [57] for calculating the vibrationally elastic and inelastic cross sections. All the calculations were carried out using the MOLSCAT computer program [60] using the propagator of Manolopoulos [61]. The reduced mass of the CN–He and CN–Ar colliding systems μ, are 3.4687 and 15.75588 amu, respectively. The integration parameters were chosen to ensure convergence of the cross sections. Numerical experiments showed that the values of the cross sections were converged to better than one per cent on including one closed (or not relevant) vibrational channel in the coupled equations. This result is in good agreement with the convergence test done for the CS-He system [62].

As in this work, we were only interested in the vibrational relaxation, the vibrational relaxation cross sections were obtained as follow :

$$\sigma(v \rightarrow v') = \sum_{j'} \sigma^{IOS}(v, j = 0 \rightarrow v', j') \tag{11}$$

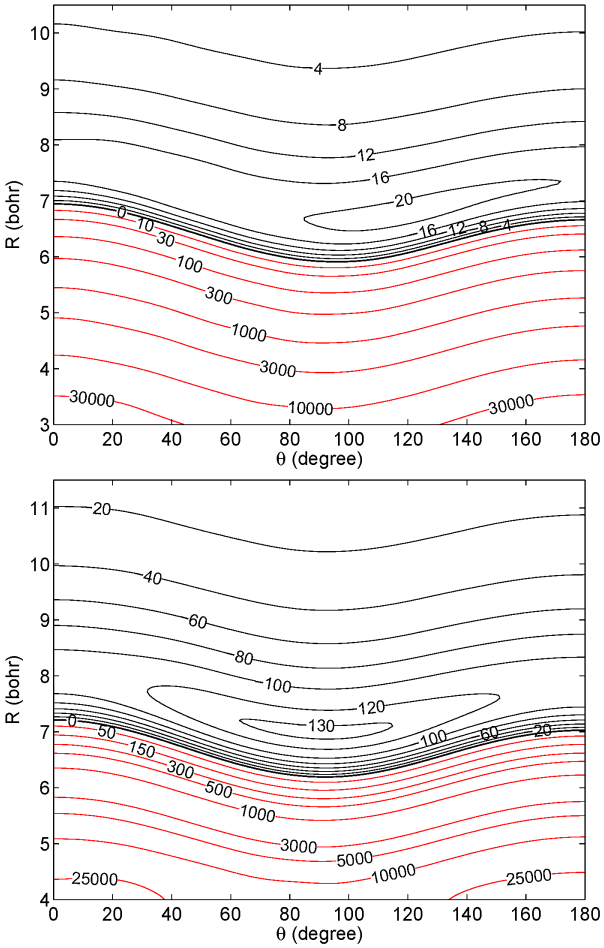

FIG. 9: Contour plot of the $V_{0,0}(R,\theta)$ matrix element of the CN–He (upper panel) and CN–Ar (lower panel) interaction potentials for vibrationally elastic scattering as a function of R and θ. The energies are in cm^{-1}.

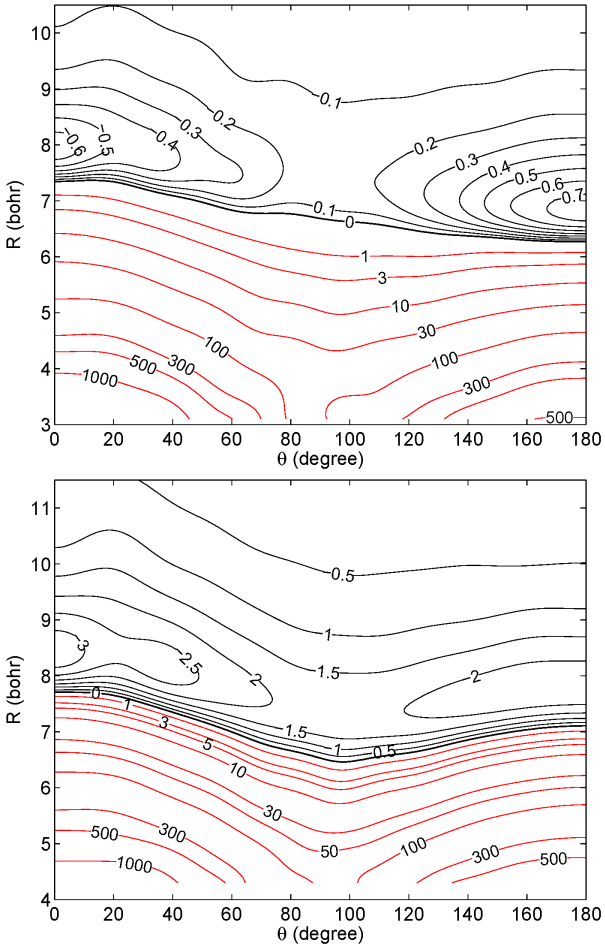

FIG. 10: Contour plot of the $V_{0,1}(R,\theta)$ matrix element of the CN–He and CN–Ar interaction potential for vibrationally inelastic scattering as a function of R and θ. The energies are in cm^{-1}.

Rate coefficients are obtained by averaging the appropriate cross sections over a Boltzmann distribution of velocities at a given kinetic temperature T :

$$k_{v\to v'} = \left(\frac{8\beta^3}{\pi\mu}\right)^{1/2} \int_0^\infty \sigma(v\to v')(E_k) \times E_k \exp\left(-\beta E_k\right) dE_k \qquad (12)$$

where $\beta = (k_B T)^{-1}$. The total energy E is related to the kinetic energy according to $E = E_k + \epsilon_v$, where ϵ_v is the energy of the initial vibrational level.

Calculations were performed for energies up to 15000 cm^{-1}. It leads to converged rate coefficients for all considered levels and temperatures up to 2000 K.

Schwartz-Slawsky-Herzfeld (SSH) empirical model

Simple model theories based on the character of the vibrational energy exchange processes in a quasi-classical approximation can be employed to give an estimate of the vibrational relaxation time. The Landau-Teller mechanism (vibration-translation energy exchange) [63] is based on the assumption that, during a collision, the vibrational transition is induced by the translational energy, and the vibrational energy is converted into the translational one. The vibrational relaxation time for the Landau-Teller mechanism is given by:

$$\tau(T,P) = \frac{1}{P} \cdot \frac{k_B T}{k_{10}\left(1-\exp(-\theta_v/T)\right)} \qquad (13)$$

where P is the pressure, k_{10} the rate coefficient of the vibrational transition, $\theta_v = \hbar/\omega_0 k_B$ the characteristic vibrational temperature with ω_0 the angular frequency. We can model the interaction between the two colliding molecules with a repulsive potential of the Born-Mayer type [64, 65]:

$$U = V_0 \exp(-\alpha R_{\text{C-N}}) \qquad (14)$$

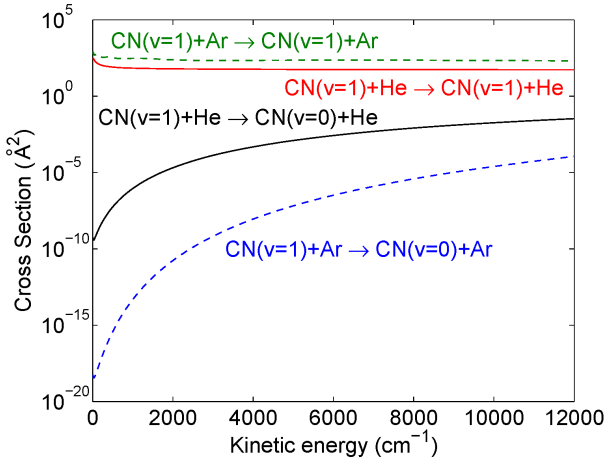

FIG. 11: Energy variation of the CN–He and CN–Ar vibrationally elastic and inelastic cross sections.

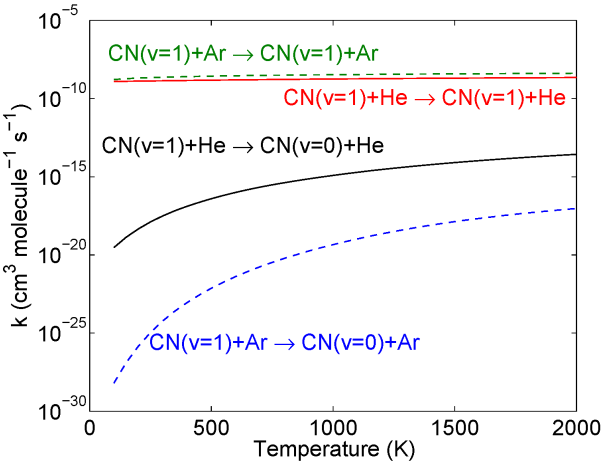

FIG. 12: Temperature variation of the CN–He and CN–Ar vibrationally elastic and inelastic rate coefficients.

The SSH model uses this mechanism to calculate the characteristic time of the vibrational relaxation. This model fits very well our case because it is applicable in the range of moderate temperatures (the Landau-Teller range: $300 \leq T \leq 3000$ K). The rate coefficient is given by [63]:

$$k_{10}(T) = S_{st} f_{at} Z_v Z_{tr} Z \tag{15}$$

where $S_{st} \sim 1/3$ is a steric factor reflecting the anisotropy of the interaction potential, f_{at} is a factor representing attraction forces, Z_v is a vibrational factor representing the coupling between the molecular vibrations and relative translational motion, Z_{tr} is a translational factor determining temperature dependence of the vibrational transition probability and Z is the gas kinetic collision frequency per unit number density.

Results of calculations

Quantum calculations of vibrationally elastic and inelastic collisions

The energy variation of the CN–He and CN–Ar vibrationally elastic and inelastic cross sections are displayed on Figure 11. For both systems, the elastic process definitely dominates the inelastic one whatever the collision energy is. This can be explained by looking at the CN–He and CN–Ar $v = 0 \rightarrow v' = 1$ potential energy matrix element for vibrationally inelastic scattering that is clearly smaller than the ones for the vibrationally elastic scattering. Then, one can see that the cross sections corresponding to the vibrational relaxation of CN($v = 1$) by Ar is much smaller by several order of magnitude than the one corresponding to the vibrational relaxation of CN($v = 1$) by He. The vibrational relaxation rate coefficients usually decreases with increasing mass of the colliding partner [66, 67], as it was already observed theoretically and experimentally for molecules such as CO [68] or CO_2 [69].

Subsequently, we used the calculated vibrationally elastic and inelastic cross sections for the CN–Ar and CN–He collisional systems to obtain, by energy averaging, the corresponding rate coefficients. Figure 12 presents the temperature variation of the CN–He and CN–Ar vibrationally elastic and inelastic rate coefficients.

The rate coefficients obviously display the same behavior than the integral cross sections. In particular, in the temperature range considered in this work, elastic process clearly dominates the inelastic one whatever the temperature is and the vibrational relaxation of CN($v = 1$) by He is much faster than the vibrational relaxation of CN($v = 1$) by Ar. One can also observe a very slow variation with temperature of the vibrationally elastic rate coefficients while the variation of the vibrational deexcitation rate coefficients vary more rapidly.

Comparison with the empirical SSH model

The empirical SSH model is employed to determine the relaxation time of CN with different partners (He, Ar, H_2 and N_2) over the 300-2000 K temperature range. The angular frequency of $\omega_0 = 2042.4073$ cm^{-1} is injected in the model. Under the current regime, the collision is slow compared to period motion and the system can be adjusted adiabatically. This corresponds to the case where the Massey parameter $\zeta = (\theta_{LT}/T)^{1/3}$ is large ($\zeta \gg 1$), with the characteristic Landau-Teller temperature θ_{LT}

given by:

$$\theta_{LT} = \frac{\pi^2 \mu \omega_0^2}{2\alpha^2 k_B}, \tag{16}$$

The most relevant observation is the difference of orders of magnitude of the relaxation time between the three carrier gases and especially with helium (See Fig. 13). Indeed, the SSH model relies on a relaxation mechanism of direct collision between the CN radical and the carrier gas. During a collision, the two partners stand out by having each part of the kinetic energy transmitted by shock and part of the internal energy of the other partner, this energy represents the vibrational energy of the vibrationally excited partner. For a collision between the CN radical and a rare gas X, if X is sufficiently heavy (i.e., the Massey parameter, ζ, is large (the case of Ar or N_2)), there will be a great impact on the center of mass of the molecule CN and the transmitted energy will be predominantly translational energy (kinetic origin), making the vibrational relaxation ineffective. If X is light (i.e. the Massey parameter is small, the case of He), the center of mass of the molecule CN barely moves and the energy of the collision is converted into vibration. The decrease of relaxation time versus temperature can be explained by the fact that at high temperatures, the collision energies are slightly larger and therefore the energy transfer becomes more efficient. This dependence is linked to ζ which has a great impact on the result since it appears in the exponential parameter Z_{tr}. The major drawback of the SSH model comes from the dependence of the calculations on the parameter α of the Born-Mayer repulsive potential. This parameter, taken as $\alpha = 3.474$ Å^{-1} for Ar and $\alpha = 2.781$ Å^{-1} for He, is involved in determining Z_v which represents the coupling between vibrational and translational motion of the CN molecule. The limitation arises from the lack of data on this parameter, usually provided by calculations of potential energy surfaces, and from errors arising from the use of an empirical formula for determining it [70].

We compare then our quantum results with those obtained from this simple empirical model. The quantum relaxation time is simply obtained by taking $(kn)^{-1}$ with n, the number density of the collisional partner. As one can see on Figure 13, there is an overall agreement between the two sets of results. It is very interesting to note that the correct order of magnitude, the correct variation with temperature is given by the SSH model. Hence, this model can be used to estimate the relaxation time of diatomic molecules in the absence of accurate experimental or theoretical data.

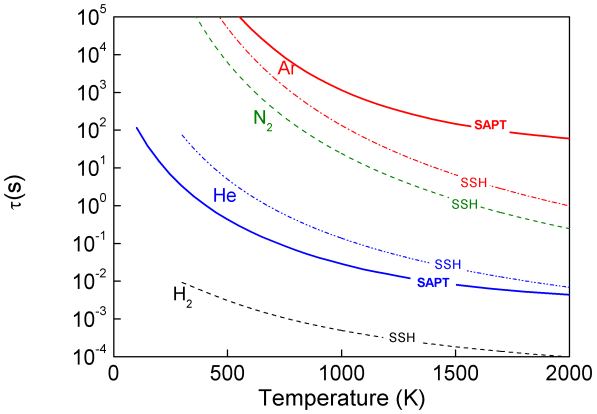

FIG. 13: Calculated characteristic $1 \rightarrow 0$ vibrational relaxation time of the CN radical with different collisional partners according to SAPT calculations (solid line) for Ar and He and to the SSH model (dotted line) for Ar, He, N_2 and H_2 for a pressure of 405 Pa.

IMPLICATIONS FOR A VARIETY OF ENVIRONMENTS

The calculated (SAPT) relaxation time of CN($v = 1$) with Ar and He versus collisional partner density and temperature is reported on Figures 14 and 15. Figure 14 clearly shows that the relaxation time of CN($v = 1$) with Ar under our experimental conditions, represented by the thick red line, never goes below 100 s. It can then unambiguously be concluded that the relaxation of CN ($v = 1$) can not significantly populate CN ($v = 0$) state under our experimental time scale a million times smaller, given by the hydrodynamic time of ~ 100 μs, and thus cannot interfere with the measurement in the high temperature flow tube. The calculations confirm that these are two distinct populations.

By contrast, the calculated relaxation time for CN($v = 1$) with He is lower by 4 to 5 orders of magnitude. It becomes then sufficiently small to compete, under certain circumstances, with other physical and chemical processes. The typical temperature and density conditions in a number of environments have been represented on Figure 15. We first examine uniform supersonic flows produced by expansion of a gas through a Laval nozzle. This type of flow is employed to perform kinetics measurements using CRESU (French acronym standing for Kinetics of Reaction in Supersonic Uniform Flows) reactors [71]. Under the conditions prevailing in CRESU helium flows ($T = 15 - 220$ K, $n = 2 \times 10^{16} - 2 \times 10^{17}$ molecule $\cdot$ cm^{-3}), the characteristic relaxation time never drops below ~ 20 s. This explains why low temperature kinetics studies of reactions involving CN [72–74] produced by UV photolysis are not disturbed by the relaxation of CN($v = 1$) which takes place on times much longer than accessible by the experiment (a few hundreds

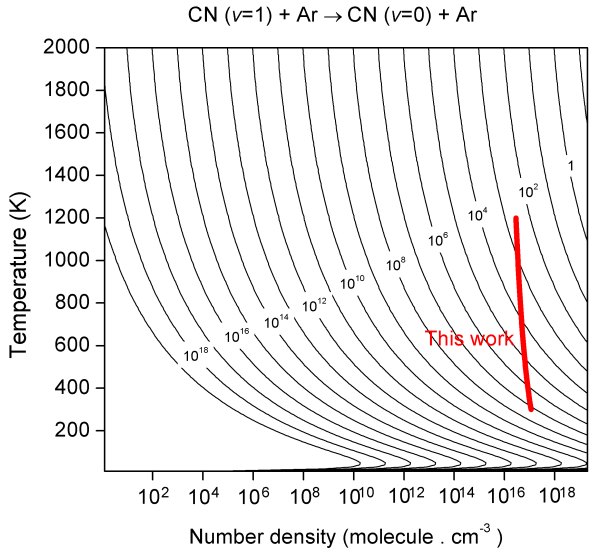

FIG. 14: Calculated relaxation time τ(s) of CN($v = 1$) with Ar vs. collisional partner number density and gas temperature. The current experimental conditions are also represented by the thick red line.

of microseconds).

The situation in combustion flames proves to be interestingly different. Replacing nitrogen in the air with argon and helium increases the range of temperature and pressure in the burners (see e.g. [75]). Assuming that He is added as a dilutent to the flame at the 0.1-0.2 level, the relaxation time falls then in the 100 μs range. This low value means that it can compete with other processes in flames. But in the absence of light collisional partners such as He, it cannot solely explain why there is no report, to our knowledge, of detection of vibrationally excited CN in flames.

The relaxation time is also reported on Figure 15 for an astrophysical object: the envelope of IRC +10216. In the envelope, CN is principally produced by photodissociation of HCN [76]. According to angular resolved studies of the Lyman-α photodissociation of HCN, the CN photofragment is formed mainly in the first excited electronic state $A^2\Pi$ in various vibrational levels in the laboratory[77]. A small percentage of the fragments is also directly produced in rovibrational states associated with CN($B^2\Sigma^+$)($v = 0, 1$). The excited CN($A^2\Pi$) and CN($B^2\Sigma^+$) radicals relax then by fluorescence in various vibrational levels of the electronic ground state $X^2\Sigma^+$. As a consequence, a fraction of CN radicals are expected to be in vibrationally excited states across the envelope. The temperature and pressure reigning in the circumstellar envelopes of evolved stars are not accurately known. Estimates strongly depend on various model assumptions, such as stellar mass loss rates, gas density outflow, and velocity. The astronomical observations have shown that the envelope of evolved stars is huge, extending over 10^4 to 10^5 stellar radii ($R_\star$), and therefore subject to strong temperature and pressure gradients. Close to the photosphere ($< 5R_\star$), the gas is dense ($n \geq 10^{10}$ molecule·cm^{-3}) and warm ($T \sim 1500$ K). As the matter flows away from the star, it expands ($n \leq 10^5$ molecule·cm^{-3}) and cools rapidly down to 25 K at several hundreds of $R_\star$. For simplicity, we use the average temperature and density analytic expressions for IRC +10216 proposed by Agúndez *et al.* [78]. Let us first examine the calculations performed for He considering an abundance of 20% of that of molecular hydrogen. Our calculations reveal that the relaxation time drops down to $\sim$ 100 s in the hottest and densest region close to the star. This low value - compared to typical time between collisions- means that collisional relaxation could represent a significant competitive channel for the destruction of CN($v = 1$) in the inner region of the envelope. However, it does not explain why CN($v = 1$) is not observed elsewhere farther out in cooler shells.

Although, the main collisional partner in this astrophysical environment is H_2, it is difficult to extend the present discussion on collision with He to the case on collision with H_2. Generally, rotational He rate coefficients can be considered as an estimate of H_2 rate coefficients in the absence of them [79]. The H_2 rate coefficients are generally higher than the He-rate coefficients by only one to a few orders of magnitude. However, in the case of vibrational relaxation of CN+H_2 collisions, the problem is more complex since no high-level calculations of vibrational relaxation rates by H_2 collisions of interstellar diatomic molecules has been performed and compared with relaxation rates due to He collisions. In addition, since CN+H_2 collisions can be reactive, it is very difficult to predict vibrational relaxation of reactive system from vibrational relaxation of non-reactive system.

However, supported by rapid calculation of the SSH model (see Figure 13), we may estimate that the rate coefficients for the CN($v = 1$) + H_2 $\rightarrow$ CN($v = 0$) + H_2 collision will be significantly larger by several orders of magnitude than the ones for the CN($v = 1$) + He $\rightarrow$ CN($v = 0$) + He relaxation. Hence, it may become a more competitive channel for the destruction of CN($v = 1$). Indeed, we note that the difference between He and H_2 relaxation times could be about 4 orders of magnitude at room temperature. This difference may even be larger at lower temperature not explored by the SSH model. Nevertheless, it would probably not be sufficient to be a really competitive channel for the destruction of CN($v = 1$) since CN is mainly observed in the coldest part of the circumstellar envelopes where the density of the gas is quite low. Hence, it seems that the absence of CN($v = 1$) cannot be explained by a fast relaxation time (from He and H_2 collisions), even if one really needs to perform accurate prediction of this relaxation time by H_2 collisions using quantum calculations.

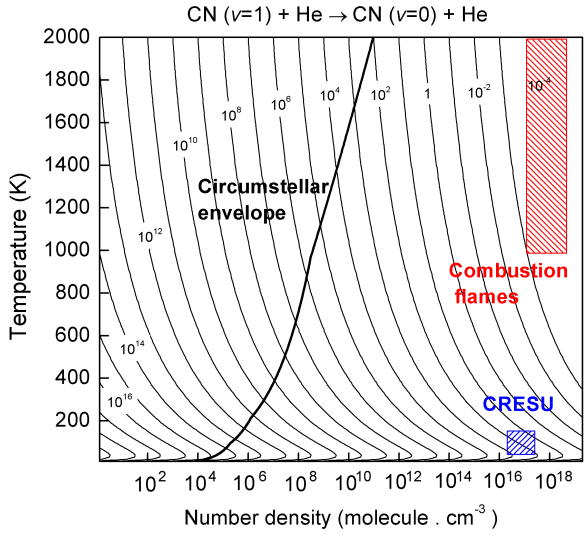

FIG. 15: Calculated relaxation time τ(s) of CN($v = 1$) with He vs. collisional partner number density and gas temperature. The conditions encountered in the circumstellar envelope of IRC +10216 (−), Fuel/Air/He combustion flames (−), and CRESU flows (−) are also reported.

The absence of CN($v = 1$) in circumstellar envelopes can neither be explained by faster reactivity of CN($v = 1$) with H_2 or hydrocarbons than the one of CN($v = 0$) as mentioned in the introduction. Another hypothesis could then simply be that vibrationally excited CN lines are very weak, and hence difficult to detect. Vibrationally excited C_2H was recently detected towards the carbon-rich envelope IRC +10216 through very weak emission lines [21]. We could expect a similar behavior for the CN molecules. Considering the high resolution and high sensitivity of the future ALMA interferometer, we expect that the mystery of non detected vibrationally excited CN will be resolved.

CONCLUSIONS

The exploration of the high temperature kinetics of neutral-neutral reactions is essential to understand and predict the formation of complex molecules in a wide range of media. In combustion flames, the reaction of CN with C_2H_6 will replenish the HCN reservoir at a fast rate whereas the CN + C_2H_4 reaction will lead to the formation of nitrile species. In circumstellar envelopes, the CN + C_2H_4 reaction can lead to molecular growth at a fast rate above 2×10^{-10} cm$^3\cdot$ molecule.$^{-1}\cdot$s^{-1} over a wide range of temperature. The reaction of CN with C_2H_4 can contribute to the formation of cyanopolyynes even in the hottest regions.

Our approach based on the use of porous material to provide a huge heat exchange surface opens the way to kinetics measurements over the 300 –2000 K window. A second generation of instruments is currently designed through careful flow dynamics calculations and chemical kinetics considerations.

From a fundamental viewpoint and in a number of extreme environments, it is imperative to identify or predict the vibrational state of the molecules in presence. The ubiquity of the CN radical makes it a good target. For these reasons, we have combined a kinetics study with quantum calculations to investigate the vibrational relaxation of CN($v = 1$), starting with simple monoatomic gases Ar and He.

In this work, we used the vibrational Close-Coupling - rotational IOS approach to investigate the vibrational energy transfer in collisions of CN with He and Ar atoms. The calculations are performed with new accurate 3D potential energy surfaces. In the energy range considered ($T \leq$2000 K) the rate coefficients for vibrational excitation are several orders of magnitude lower than the vibrationally elastic rate coefficients. As a consequence, vibrational relaxation of CN by He and especially Ar may be considered as negligible process in kinetics simulations as well as in astrophysical environments and combustion midfield.

We also found that the SSH model was able to predict the correct order of magnitude of relaxation rate coefficients. This finding is very investing for future kinetic studies. Indeed, accurate theoretical calculations of relaxation rate coefficients of diatomic molecule by collisions with diatomic molecule such as N_2 or H_2 are very complex to study from both the quantum chemistry and dynamical calculations points of view. If one could estimate these data using the relatively simple SSH model, it would be very helpful for analyzing kinetic experiments as well as kinetics of energized media.

We express our gratitude to Bertrand Rowe for the experimental design, Jonathan Courbe for the mechanical design and Daniel Travers for the data acquisition. We thank Andrei Vigasin for helpful discussions regarding the empirical model. We are thankful to Rafal Podezswa for useful discussions on *ab initio* calculations. We thank Jose Cernicharo and Marcelino Agúndez for their insights on the chemistry of CN in IRC +10216. This research was supported by the CNRS national programs of *Physique et Chimie du Milieu Interstellaire* and of *Physique Stellaire*. R.G. and L.B acknowledge support from the Indo-French Centre for the Promotion of Advanced Research (IFCPAR). We also thank the CPER Haute- Normandie/CNRT/Energie, Electronique, Matériaux. *Ab initio* calculations were performed using HPC resources of SKIF-Cyberia (Tomsk State University).

[1] J. A. Miller and C. T. Bowman, Progress in Energy and Combustion Science **15**, 287 (1989).

[2] X. Mercier, L. Pillier, J.-F. Pauwels, and P. Desgroux, Comptes Rendus de l'Académie des Sciences - Series IV - Physics **2**, 965 (2001).

[3] J. Luque, J. Jeffries, G. Smith, D. Crosley, and J. Scherer, Combustion and Flame **126**, 1725 (2001).

[4] H. Olofsson, in *Proceedings of The dusty and molecular universe: a prelude to Herschel and ALMA*, edited by A. Wilson (2005), pp. 223–228.

[5] M. Guélin, R. Lucas, and R. Neri, in *IAU Symposium*, edited by W. B. Latter, S. J. E. Radford, P. R. Jewell, J. G. Mangum, and J. Bally (1997), vol. 170 of *IAU Symposium*, pp. 359–366.

[6] V. Wakelam, E. Herbst, J.-C. Loison, I. W. M. Smith, V. Chandrasekaran, B. Pavone, N. G. Adams, M.-C. Bacchus-Montabonel, A. Bergeat, K. Béroff, et al., The Astrophysical Journal Supplement Series **199**, 21 (2012).

[7] A. Dayal and J. H. Bieging, The Astrophysical Journal **439**, 996 (1995).

[8] E. Herbst and C. M. Leung, Astronomy and Astrophysics **233**, 177 (1990).

[9] A. Gardez, G. Saidani, L. Biennier, R. Georges, E. Hugo, V. Chandrasekaran, V. Roussel, B. Rowe, K. P. J. Reddy, and E. Arunan, International Journal of Chemical Kinetics **44**, 753 (2012).

[10] I. R. Sims and I. W. M. Smith, Chemical Physics Letters **149**, 565 (1988).

[11] I. R. Sims and I. W. M. Smith, J. Chem. Soc., Faraday Trans. 2 **85**, 915 (1989).

[12] V. Lozovsky, I. Derzy, and S. Cheskis, Chemical Physics Letters **284**, 407 (1998).

[13] T. Zhang, X. N. Tang, K.-C. Lau, C. Y. Ng, C. Nicolas, D. S. Peterka, M. Ahmed, M. L. Morton, B. Ruscic, R. Yang, et al., J. Chem Phys. **124**, 074302 (2006).

[14] J. J. Keady, D. N. B. Hall, and S. T. Ridgway, The Astrophysical Journal **326**, 832 (1988).

[15] N. A. Patel, K. H. Young, S. Brünken, K. M. Menten, P. Thaddeus, and R. W. Wilson, The Astrophysical Journal Letters **691**, L55 (2009).

[16] B. E. Turner, Astronomy and Astrophysics **182**, L15 (1987).

[17] J. L. Highberger, A. J. Apponi, J. H. Bieging, L. M. Ziurys, and J. G. Mangum, Astrophysical Journal **544**, 881 (2000).

[18] B. E. Turner, Astronomy and Astrophysics **183**, L23 (1987).

[19] J. J. Keady and S. T. Ridgway, The Astrophysical Journal **406**, 199 (1993).

[20] J. Cernicharo, M. Agúndez, C. Kahane, M. Guélin, J. R. Goicoechea, N. Marcelino, E. De Beck, and L. Decin, Astronomy and Astrophysics **529**, L3 (2011).

[21] E. D. Tenenbaum, J. L. Dodd, S. N. Milam, N. J. Woolf, and L. M. Ziurys, The Astrophysical Journal Letters **720**, L102 (2010).

[22] A. Moudens, R. Georges, A. Benidar, B. Amyay, M. Herman, A. Fayt, and B. Plez, Journal of Quantitative Spectroscopy and Radiative Transfer **112**, 540 (2011).

[23] J. Thiévin, R. Georges, S. Carles, A. Benidar, B. Rowe, and J.-P. Champion, Journal of Quantitative Spectroscopy and Radiative Transfer **109**, 2027 (2008).

[24] L. Biennier, R. Georges, V. Chandrasekaran, B. Rowe, T. Bataille, V. Jayaram, K. P. J. Reddy, and E. Arunan, Carbon **47**, 3295 (2009).

[25] J. Luque and D. R. Crosley, Tech. Rep. Report MP 96-001, SRI International (1996).

[26] A. Baronavski, Chemical Physics **66**, 217 (1982).

[27] J. A. Myer and J. A. R. Samson, The J. Chem Phys. **52**, 266 (1970).

[28] D. L. Yang, T. Yu, N. S. Wang, and M. C. Lin, Chemical Physics **160**, 307 (1992).

[29] W. P. Hess, J. L. Durant, and F. P. Tully, The Journal of Physical Chemistry **93**, 6402 (1989).

[30] L. Herbert, I. W. M. Smith, and R. D. Spencer-smith, International Journal of Chemical Kinetics **24**, 791 (1992).

[31] R. J. Balla, K. H. Casleton, J. S. Adams, and L. Pasternack, Journal of Physical Chemistry **95**, 8694 (1991).

[32] L. R. Copeland, F. Mohammad, M. Zahedi, D. H. Volman, and W. M. Jackson, J. Chem Phys. **96**, 5817 (1992).

[33] B. Atakan and J. Wolfrum, Chemical Physics Letters **186**, 547 (1991).

[34] G. E. Bullock and R. Cooper, J. Chem. Soc. Faraday Trans. 1 **68**, 2185 (1972).

[35] I. R. Sims, J.-L. Queffelec, D. Travers, B. R. Rowe, L. B. Herbert, J. Karthäuser, and I. W. M. Smith, Chemical Physics Letters **211**, 461 (1993).

[36] Y. Georgievskii and S. J. Klippenstein, The Journal of Physical Chemistry A **111**, 3802 (2007).

[37] Y. Georgievskii and S. J. Klippenstein, The J. Chem Phys. **122**, 194103 (2005).

[38] E. E. Greenwald, S. W. North, Y. Georgievskii, and S. J. Klippenstein, The Journal of Physical Chemistry A **109**, 6031 (2005).

[39] N. Choi, M. A. Blitz, K. McKee, M. J. Pilling, and P. W. Seakins, Chemical Physics Letters **384**, 68 (2004).

[40] A. Albernaz, R. Gargano, P. Barreto, and N. Balucani, in *Computational Science and Its Applications (ICCSA), 12th International Conference on* (2012), pp. 57 –62.

[41] P. S. Monks, P. N. Romani, F. L. Nesbitt, M. Scanlon, and L. J. Stief, J. Geophys. Res. **98**, 17115 (1993).

[42] N. Balucani, O. Asvany, A. H. H. Chang, S. H. Lin, Y. T. Lee, R. I. Kaiser, and Y. Osamura, J. Chem Phys. **113**, 8643 (2000).

[43] D. A. Lichtin and M. C. Lin, Chemical Physics **104**, 325 (1986).

[44] P. S. Ĭuchowski et al., J. Chem. Phys. **129**, 084101 (2008).

[45] R. Bukowski, W. Cencek, P. Jankowski, M. Jeziorska, B. Jeziorski, S. A. Kucharski, V. F. Lotrich, A. J. Misquitta, R. Moszyński, K. Patkowski, et al., *SAPT2008: An* ab initio *program for many-body symmetry-adapted perturbation theory calculations of intermolecular interaction energies*, University of Delaware and University of Warsaw (2008), URL `http://www.physics.udel.edu/~szalewic/SAPT/SAPT.html`.

[46] C. Adamo and V. Barone, J. Chem. Phys. **110**, 6158 (2001).

[47] A. J. Misquitta and K. Szalewicz, J. Chem. Phys. **122**, 214109 (2005).

[48] A. J. Misquitta and K. Szalewicz, J. Chem. Phys. **123**, 214103 (2005).

[49] H. L. Williams, E. M. Mass, K. Szalewicz, and B. Jeziorski, J. Chem. Phys. **103**, 7374 (1995).

[50] T. H. Dunning, J. Chem. Phys. **90**, 1007 (1989).

[51] R. Podeszwa, R. Bukowski, and K. Szalewicz, J. Chem.

Theory Comput. **2**, 400 (2006).
[52] J. Rezac and P. Hobza, J. Chem. Theory Comput. **7**, 685 (2011).
[53] F. Lique, A. Spielfiedel, N. Feautrier, I. F. Schneider, J. Kłos, and M. H. Alexander, J. Chem. Phys. **132**, 024303 (2010).
[54] R. Moszynski, B. Jeziorski, S. Rybak, K. Szalewicz, and H. L. Williams, J. Chem. Phys. **100**, 5080 (1994).
[55] K. S. K. Patkowski, R. Podeszwa, J. Phys. Chem. A **111**, 12822 (2007).
[56] H.-J. Werner, B. Follmeg, and M. H. Alexander, J. Chem. Phys. **89**, 3139 (1988).
[57] G. A. Parker and R. T. Pack, J. Chem. Phys. **68**, 1585 (1978).
[58] C. Clay Marston and G. G. Balint-Kurti, J. Chem. Phys. **91**, 3571 (1989).
[59] J. Han, M. C. Heaven, U. Schnupf, and M. H. Alexander, J. Chem. Phys. **128**, 104308 (2008).
[60] J. M. Hutson and S. Green (1994), MOLSCAT computer code, version 14 (1994), distributed by Collaborative Computational Project No. 6 of the Engineering and Physical Sciences Research Council (UK).
[61] D. E. Manolopoulos, J. Chem. Phys. **85**, 6425 (1986).
[62] F. Lique and A. Spielfiedel, Astron. Astrophys. **462**, 1179 (2007).
[63] G. Chernyi, S. Losev, S. Macheret, and B. Potapkin, *Physical and Chemical Process in Gas Dynamics: Cross Sections and Rate Constants*, vol. 196 (American Institute of Aeronautics and Astronautics, 1995).
[64] A. A. Abrahamson, Physical Review **178**, 76 (1969).
[65] V. I. Gaydaenko and V. K. Nikulin, Chemical Physics Letters **7**, 360 (1970).
[66] R. C. Millikan and D. R. White, J. Chem. Phys. **39**, 3209 (1963).
[67] R. C. Millikan, J. Chem. Phys. **40**, 2594 (1964).
[68] R. Schinke and G. H. F. Diercksen, J. Chem. Phys. **83**, 4516 (1985).
[69] F. Lepoutre, G. Louis, and J. Taine, J. Chem. Phys. **70**, 2225 (1979).
[70] A. Lifshitz, The J. Chem Phys. **61**, 2478 (1974).
[71] B. R. Rowe, G. Dupeyrat, J. B. Marquette, and P. Gaucherel, J. Chem Phys. **80**, 4915 (1984).
[72] I. R. Sims, J. L. Queffelec, A. Defrance, C. Rebrion-Rowe, D. Travers, P. Bocherel, B. R. Rowe, and I. W. M. Smith, J. Chem Phys. **100**, 4229 (1994), dOI: 10.1063/1.467227.
[73] S. B. Moralès, S. D. Le Picard, A. Canosa, and I. R. Sims, Faraday Discussions **147**, 155 (2010).
[74] S. B. Moralès, C. J. Bennett, S. D. Le Picard, A. Canosa, I. R. Sims, B. J. Sun, P. H. Chen, A. H. H. Chang, V. V. Kislov, A. M. Mebel, et al., The Astrophysical Journal **742**, 26 (2011).
[75] K. Eisazadeh-Far, A. Moghaddas, H. Metghalchi, and J. C. Keck, Fuel **90**, 1476 (2011).
[76] M. Lindqvist, F. Schoier, R. Lucas, and H. Olofsson, Astronomy and Astrophysics **361**, 1036 (2000).
[77] P. A. Cook, S. R. Langford, M. N. R. Ashfold, and R. N. Dixon, J. Chem Phys. **113**, 994 (2000).
[78] M. Agúndez, J. P. Fonfría, J. Cernicharo, C. Kahane, F. Daniel, and M. Guélin, Astronomy & Astrophysics **543**, A48 (2012).
[79] F. Lique, R. Toboła, J. Kłos, N. Feautrier, A. Spielfiedel, L. F. M. Vincent, G. Chałasiński, and M. H. Alexander, A&A **478**, 567 (2008).
[80] http://scienide2.uwaterloo.ca/ rleroy/rkr/